PNAS

Supporting Information for
Local and dynamic regulation of neuronal glycolysis *in vivo*

Aaron D. Wolfe, John N. Koberstein, Chadwick B. Smith, Melissa L. Stewart, Ian J. Gonzalez, Marc Hammarlund, Anthony A. Hyman, Philip J.S. Stork, Richard H. Goodman, Daniel A. Colón-Ramos

Richard H. Goodman
Email: rgoodman@ohsu.edu

Daniel A. Colón-Ramos
Email: daniel.colon-ramos@yale.edu

This PDF file includes:

Figures S1 to S4
Table S1
Legends for Movies S1 to S2
SI References

Other supporting materials for this manuscript include the following:

Movies S1 to S2

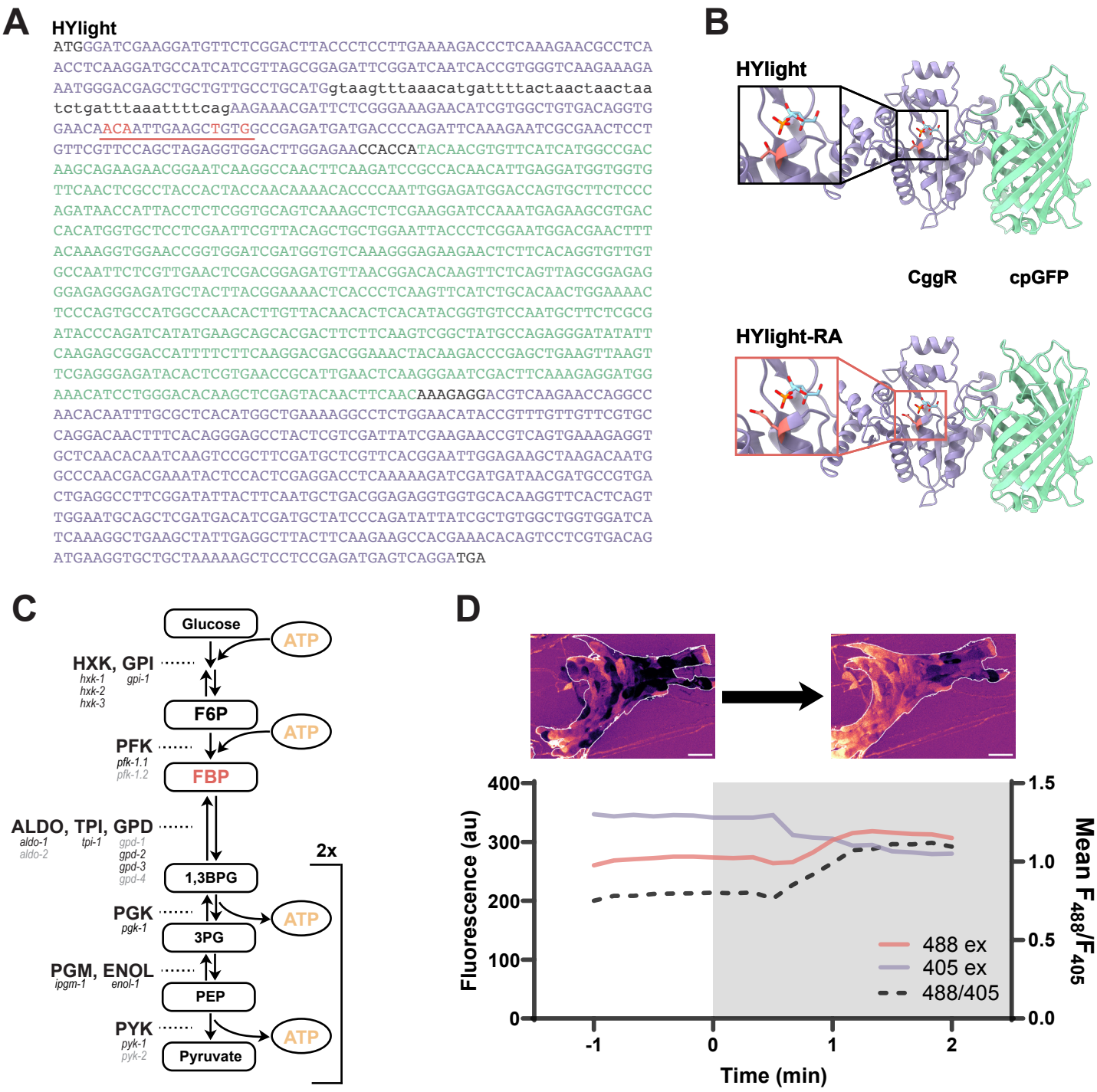

Figure S1. The HYlight biosensor measures FBP inside cells of *C. elegans*. **(A)** DNA sequence of the sensor HYlight(1) adapted for expression in *C. elegans*. HYLight is comprised of a fusion between cpGFP and the Central Glycolytic Gene Regulator (CggR), a transcriptional regulator of metabolism from *Bacillus subtilis*. The CggR regions are shown in purple; cpGFP is shown in green. The inserted intron at the 5' end is shown in lowercase bases. To generate HYlight-RA , threonine 152 (in CggR numbering) is mutated to glutamate in the red underlined region. The corresponding sequence in the

HYlight-RA construct is 5'...GAGATTGAAGCAGTT...3', where the red nucleotides represent those that are changed. The two silent mutations which are also present were added to improve cloning efficiency. **(B)** Structure models of HYlight compared to HYlight-RA. The model of HYlight was generated with AlphaFold2(2, 3), and the bound F6P molecule (see inset) was placed by aligning the crystal structure of CggR bound to FBP from RCSB ID 3BXF(4). The residue important for binding to FBP that is mutated in HYlight-RA is shown in red, with the glutamate mutation shown below (red inset). **(C)** Diagram of glycolysis, showing known homologs of each gene that are present in *C. elegans*. Genes that are less ubiquitously expressed in neurons based on scRNA-SEQ data(5) are shown in light grey. The location of FBP within the pathway is highlighted in red. **(D)** The ratiometric nature of HYlight is due to the opposite responses of each excitation wavelength to the current level of FBP; this effect is also seen *in vivo*. Initially, when FBP is low, the 488 nm excitation strength is lower than for 405 nm, resulting in a low ratio of 488/405 seen in most cells. Upon hypoxia, this ratio increases due to a reversal in intensity strength: the 488 nm excitation is now higher than 405 nm. Chart represents the mean intensity across all neurons at each time point of a representative dataset; inset images are max projection representations of the first frame (at -1 minute) and last frame (at +2 minutes after hypoxia onset). Scale bars represent 10 μm.

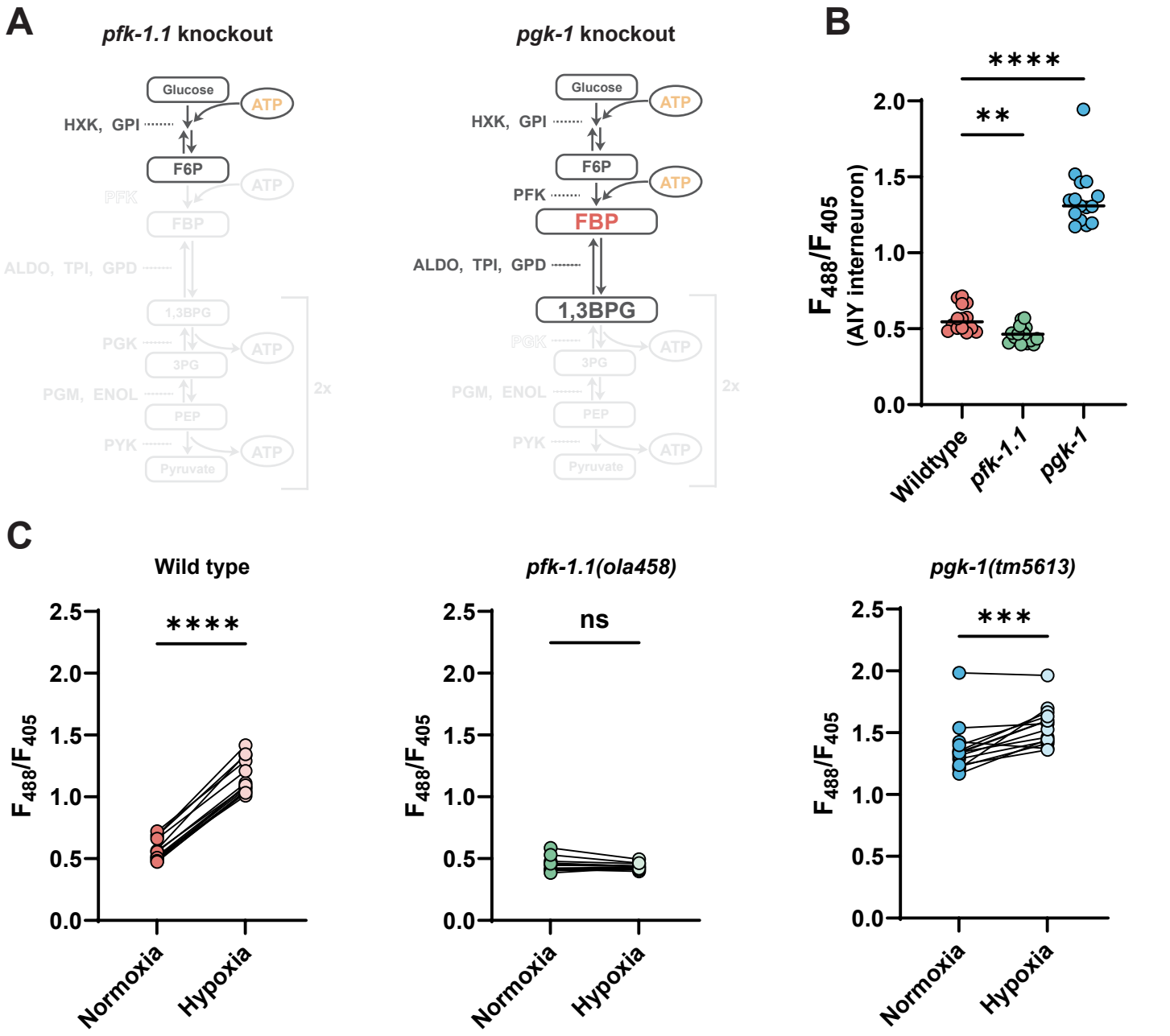

Figure S2. Genetic manipulation of FBP levels in *C. elegans*. **(A)** Schematic of the glycolytic pathway and expected affected steps for examined mutants. Mutation of the gene *pfk-1.1*, which catalyzes the conversion of F6P to FBP, should result in a near-complete elimination of FBP in cells (left), as they lack any alternative production pathway for the molecule. Conversely, loss of the gene *pgk-1* (right), which catalyzes a downstream reaction step converting 1,3BPG into 3PG, should result in an accumulation of FBP, as reduced usage would cause the reversible reactions between PFK and PGK to reach an elevated equilibrium value. **(B)** Measurement of HYlight ratios in the interneuron AIY for the indicated genetic backgrounds. Compa red to wild-type worms, the *pfk-1.1(ola458)* mutant background

results in a significantly reduced HYlight ratio (P-value: 0.0032) whereas the *pgk-1(tm5613)* mutant results in a significantly elevated ratio compared to wild type (P-value: <0.0001), as expected based on their position in the glycolytic pathway. Significance calculated by ANOVA with Tukey post-hoc test for multiple comparisons for 15 animals. **(C)** Effects of hypoxia treatment in different glycolytic mutants. Wild-type worms show a significantly higher ratio after treatment with hypoxia compared to the starting ratio within individual cells (P-value: <0.0001). In contrast, *pfk-1.1(ola458)* worms showed no significant change in the ratio upon hypoxia treatment (P-value: 0.1571). Worms with the *pgk-1(tm5613)* mutant background do see a significant increase upon hypoxia (P-value: 0.0003), despite starting at an elevated ratio. Values calculated as the mean value within a 30 second window between -1 minute to -30 seconds before hypoxia, and between 2:15 to 2:45 after hypoxia exposure begins, which roughly reflect the initial value and the peak increase in glycolysis for wild type, respectively. Significance calculated as a 2-tailed paired t-test for before and after hypoxia treatment per worm.

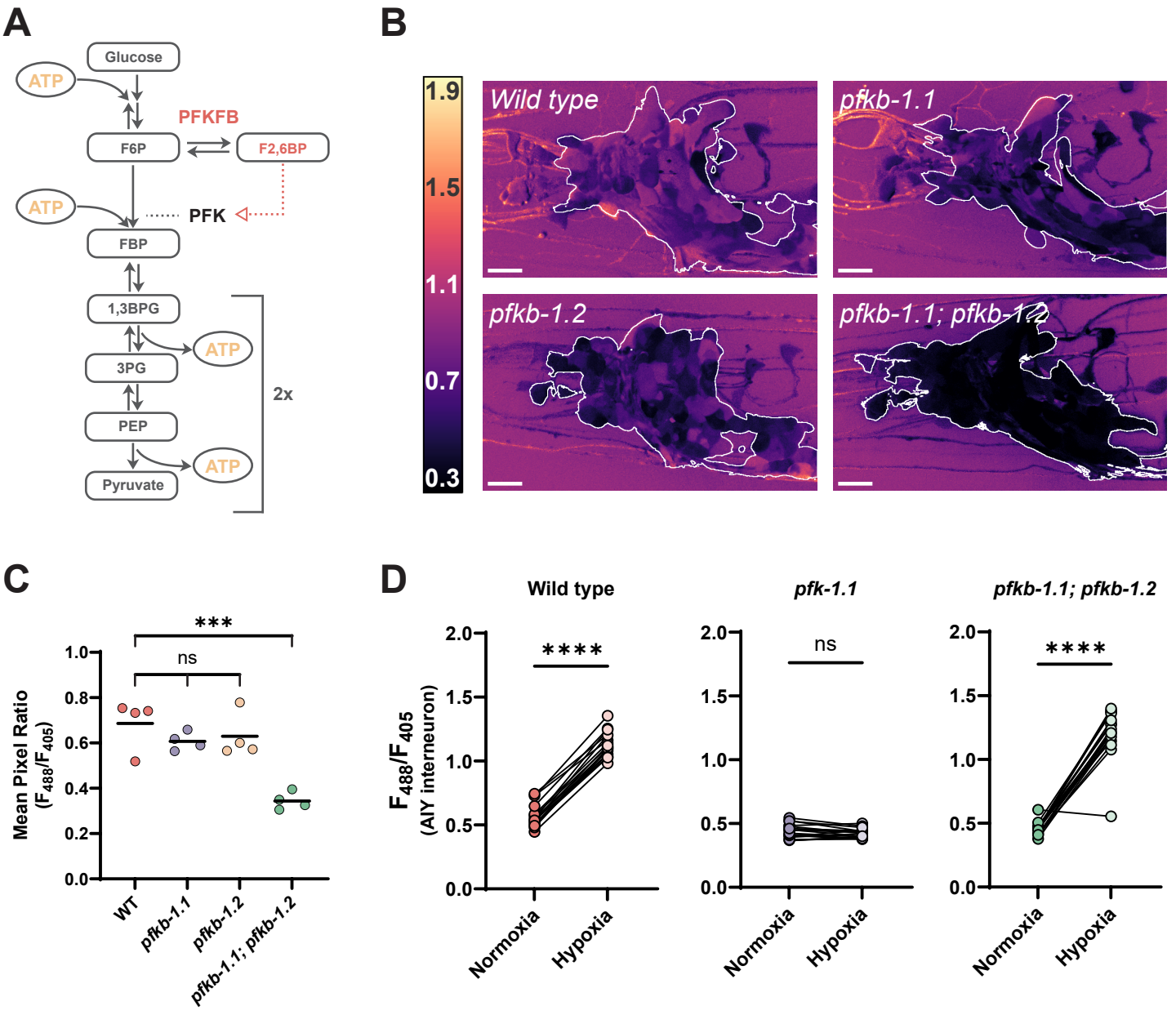

Figure S3. The two homologs of PFKFB, *pfkb-1.1* and *pfkb-1.2*, are functionally redundant in regulating neuronal glycolysis in *C. elegans*. **(A)** Visualization of the glycolytic pathway with role of PFKFB shown. PFKFB enzymes interconvert F6P and F2,6BP, a potent activator of the enzyme PFK. Activation of PFK is depicted by the red, dashed line with open arrowhead. **(B)** Images of pan-neuronal HYlight expression in either wild-type, *pfkb-1.1(ok 2733)* mutant, *pfkb-1.2(ola508)* mutant or *pfkb-1.1; pfkb-1.2* double mutant backgrounds. Images of wild type and the double mutant are also shown in Figure 3 of this paper. Scale bars reflect 10 μm. White outlines depict the ROIs used for quantification of mean ratio for each worm. **(C)** Quantification of HYlight values for indicated genetic backgrounds. Each dot represents individual animals. P-values shown are 0.529 (WT vs. *pfkb-1.1*), 0.750 (WT vs.

pfkb-1.2), 0.980 (*pfkb-1.1* vs. *pfkb-1.2)*, and 0.0003 (WT vs. *pfkb-1.1; pfkb-1.2)*. Significance calculated by ANOVA with Tukey post-test for multiple comparisons across 4 individual worms of at least 60 Z slices. **(D)** Quantification of the effect of hypoxia in different mutant backgrounds in the AIY interneurons. Wild-type worms see a statistically significant increase in mean ratio upon hypoxia treatment (P-value: <0.0001), whereas *pfk-1.1(ola458)* mutant worms see no significant change (P-value: 0.1442). The *pfkb-1.1(ok2733); pfkb-1.2(ola508)* double mutant worms also see a significant increase upon hypoxia (P-value: <0.0001). Significance calculated for each genotype by comparing the mean ratio within the first 30 seconds of experiment and between 2:15 and 2:45 after hypoxia treatment per each worm using a two-tailed paired t-test. Data is replotted from Figure 3G.

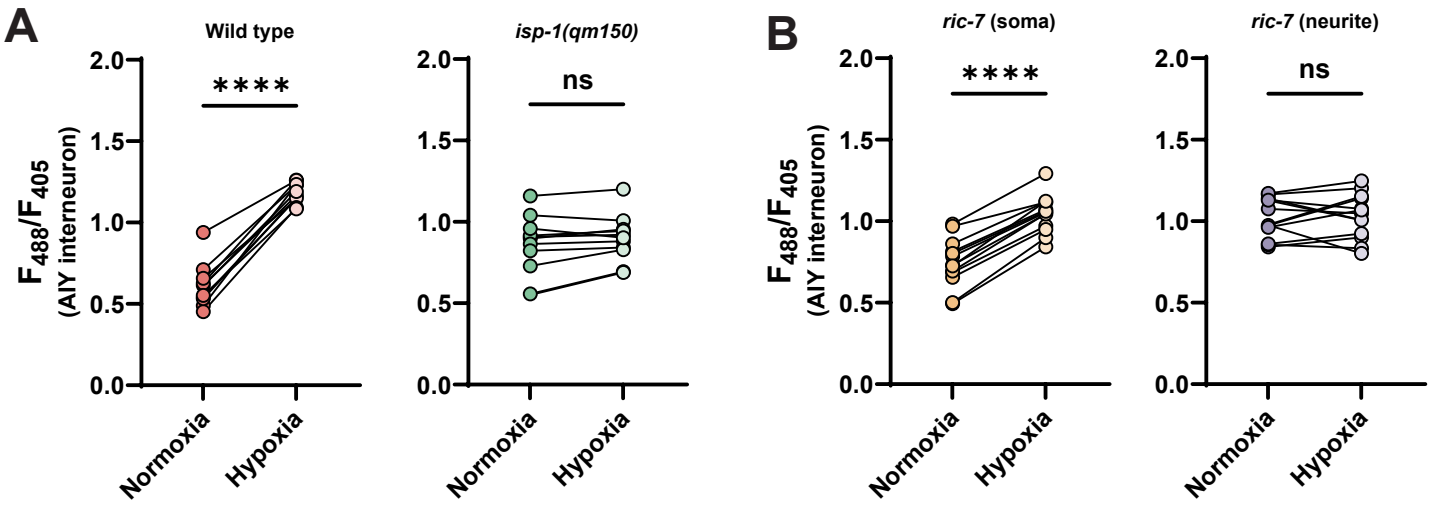

Figure S4. Effect of hypoxia in backgrounds of mitochondrial mutants. **(A)** Worms with defective mitochondria do not respond to hypoxia. Wild-type worms show a statistically significant increase in mean ratio upon hypoxia exposure (P-value: <0.0001), whereas the *isp-1(qm150)* mutant background sees no change in the mean glycolytic ratio upon hypoxia (P-value: 0.0508). Signicance determed as a two-tailed paired t-test per worm. Data from Figure 4A, replotted to show the effect of hypoxia. **(B)** In a *ric-7(n2657)* mutant background, there are subcellular differences in the effects of hypoxia. In the cell soma, where mitochondria are located, there is a significant increase in the observed ratio after hypoxia treatment (P-value: <0.0001), whereas in the neurite this increase is not observed (P-value: 0.7091). Signicance determed as a two-tailed paired t-test per worm. Data from Figure 4E, replotted to show the effect of hypoxia.

Table S1. List of strains used within this study.

Strain	Genotype	Source
N2	Bristol wild-type strain	CGC
DCR3373	*olaEx1951 [ttx-3p::tom-20:GFP; ttx-3p::mCherry:rab-3]*	(6)
DCR8881	*olaEx5329 [rab-3p::HYlight]*	This study
DCR8892	*olaEx5331 [rab-3p::HYlight-RA]*	This study
DCR8981	*olaEx5367 [ttx-3p::HYlight]*	This study
DCR9016	*pfk-1.1(ola458); olaEx5329*	This study
DCR9089	*olaIs138 [ttx-3p::HYlight] IV*	This study
DCR9164	*olaEx5443 [unc-47p::HYlight]*	This study
DCR9168	*pgk-1(tm5613) I; olaIs138 IV*	This study
DCR9169	*pfkb-1.1(ok2733) I; pfkb-1.2(ola508) IV; olaEx5367*	This study
DCR9197	*olaIs138 IV; pfk-1.1(ola458) X*	This study
DCR9218	*olaIs138 IV; pfk-1.1(ola458) X; olaEx5468 [ttx-3p::SL2::pfk-1.1]*	This study
DCR9238	*pfkb-1.2(ola508) olaIs138 IV*	This study
DCR9251	*pfkb-1.1(ok2733) I; olaIs138 IV*	This study
DCR9358	*pfkb-1.1(ok2733) I; pfkb-1.2(ola508) IV; olaEx5329*	This study
DCR9359	*pfkb-1.1(ok2733) I; olaEx5329*	This study
DCR9360	*pfkb-1.2(ola508) IV; olaEx5329*	This study
DCR9421	*pfkb-1.1(ok2733) I; pfkb-1.2(ola508) IV; olaEx5443*	This study
DCR9422	*ric-7(n2657) V; olaEx1951*	This study
DCR9442	*isp-1(qm150) IV; olaEx5367*	This study
DCR9443	*olaIs138 IV; ric-7(n2657) V.*	This study
EG8040	*oxTi302 I; oxTi75 II; oxTi411 unc-119(ed3) III; him-8(e1489) IV*	CGC
XE1763	*oxTi76 IV; oxTi405 him-5(e1490) V; oxIs12 X*	Gift (M.H.)

Movie S1 (separate file). HYlight response in neurons upon treatment with hypoxia. A single worm expressing pan-neuronal HYlight (*rab-3p)* was mounted on a microfluidics device (for applying transient hypoxia) as described in Methods. Frames were captured as 2-channel 25 µm Z stacks with 0.5 µm spacing every 30 seconds at 60x magnification. The first minute was captured in the presence of air; at time zero, the flow was switch to N2 gas, which then subsequently was captured for an additional 9 minutes.

Movie S2 (separate file). HYlight responses in AIY neurons upon treatment with hypoxia. Multiple worms expressing HYlight in the AIY neurons (*ttx-3p*) were imaged at lower magnification while experiencing transient hypoxia, as described in Methods. After an initial 1-minute treatment with air, a switch to N2 gas was performed (time 0) and images were captured for the remainder of the experiment in hypoxia. Images were captured every 5 seconds at a single Z plane at 10x magnification. Shown is a crop to 300 x 300 pixels with grayscale values for 405 excitation fluorescence on left and ratiometric HYlight (488/405) at right. Scale bar reflects 20 µm.

SI References

1. J. N. Koberstein, *et al.*, Monitoring glycolytic dynamics in single cells using a fluorescent biosensor for fructose 1,6-bisphosphate. *Proc. Natl. Acad. Sci.* **119**, e2204407119 (2022).

2. J. Jumper, *et al.*, Highly accurate protein structure prediction with AlphaFold. *Nature* **596**, 583–589 (2021).

3. M. Mirdita, *et al.*, ColabFold: making protein folding accessible to all. *Nat. Methods* **19**, 679–682 (2022).

4. P. Řezáčová, *et al.*, Crystal structures of the effector-binding domain of repressor Central glycolytic gene Regulator from Bacillus subtilis reveal ligand-induced structural changes upon binding of several glycolytic intermediates. *Mol. Microbiol.* **69**, 895–910 (2008).

5. S. R. Taylor, *et al.*, Molecular topography of an entire nervous system. *Cell* **184**, 4329-4347.e23 (2021).

6. S. E. Hill, *et al.*, Maturation and Clearance of Autophagosomes in Neurons Depends on a Specific Cysteine Protease Isoform, ATG-4.2. *Dev. Cell* **49**, 251-266.e8 (2019).